Supplemental material

Nagase et al., https://doi.org/10.1084/jem.20171151

Table S1 is provided as an Excel file and shows motif enrichment analysis of Aszl1 mutant– and Asxl-WT–binding sites.

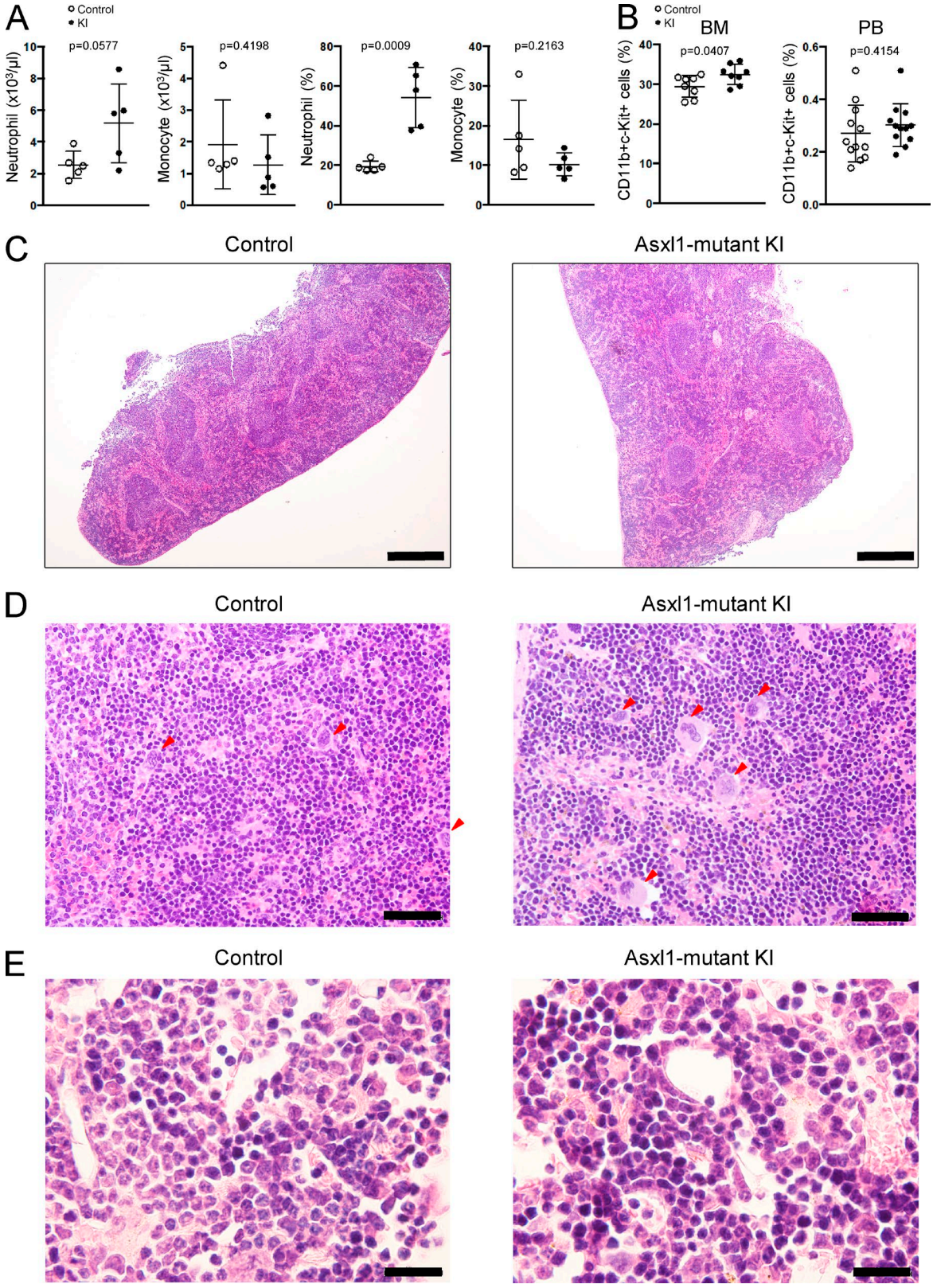

Figure S1. **Characterization of KI mice. (A)** The absolute number and frequency of neutrophil and monocyte in PB of primary *Vav*-Cre–negative *Asxl1*-MT$^{fl/fl}$ (control, 70 wk old, white circle, $n = 5$) and *Vav*-Cre–positive *Asxl1*-MT$^{fl/fl}$ mice (KI, 70 wk old, black circle, $n = 5$). **(B)** The frequency of CD11b$^+$/c-Kit$^+$ cells in whole BM cells and PB of primary *Vav*-Cre–negative *Asxl1*-MT$^{fl/fl}$ (control, 12 wk old, white circle; BM, $n = 8$; PB, $n = 12$) and *Vav*-Cre–positive *Asxl1*-MT$^{fl/fl}$ mice (KI, 12 wk old, black circle; BM, $n = 8$; PB, $n = 12$). Data are presented as mean ± SEM. **(C–E)** Histological findings in spleen (C and D) and BM (E). 70-wk-old *Vav*-Cre–negative *Asxl1*-MT$^{fl/fl}$ mice (control) and *Vav*-Cre–positive *Asxl1*-MT$^{fl/fl}$ mice (*Asxl1*-MT KI) were used. Red arrows indicate megakaryocytes (D). Bars: 500 μm (C), 50 μm (D), and 20 μm (E).

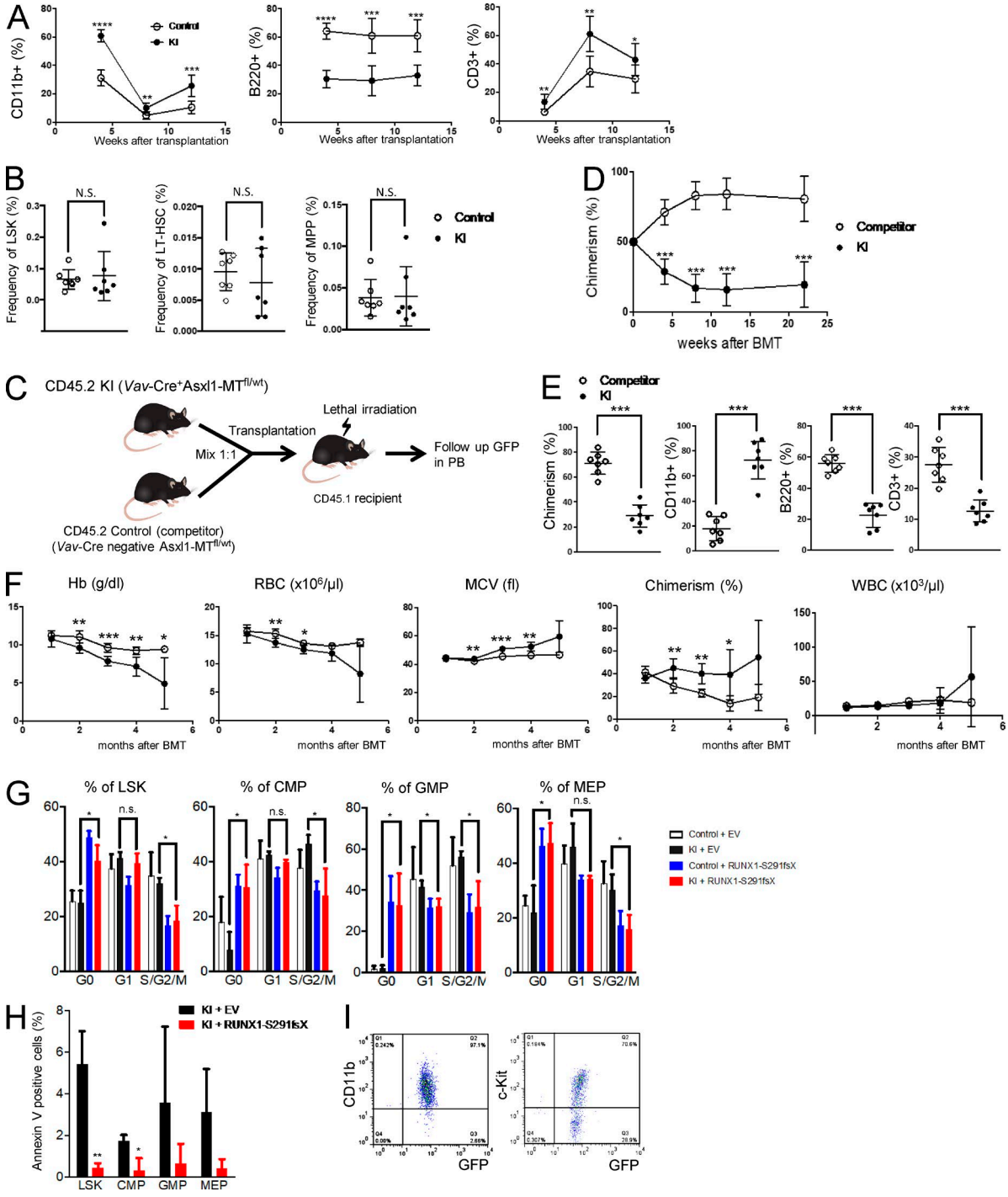

Figure S2. **Characterization of HSC and progenitor fractions. (A)** CD11b⁺/B220⁺/CD3⁺ cells in the PB were followed every 4 wk after transplantation (related to Fig. 4, A and B). **(B)** Frequency of donor-derived LSK, LT-HSCs, and MPPs in whole BM cells is shown (n = 7 each; related to Fig. 4, C and D). **(C)** Schematic depiction of another competitive transplantation assay. *Vav*-Cre–negative *Asxl1*-MT$^{fl/wt}$ (competitor) and *Vav*-Cre–positive *Asxl1*-MT$^{fl/wt}$ (KI) mice are positive for CD45.2. Recipient mice are positive for CD45.1. Unfractionated BM cells (0.5×10^6) from competitor and KI (mixed 1:1) mice were transplanted into lethally irradiated (9.5 Gy) recipients (n = 7 mice per group). **(D and E)** Chimerism (GFP⁺; D) and CD11b⁺/B220⁺/CD3⁺-positive cells (E) in the PB were studied (n = 7 each). The percentage of each lineage at 4 wk after transplantation is shown (E). **(F)** Follow-up analysis of the PB in hemoglobin (Hb), RBCs, MCV, chimerism, and WBCs in mice transplanted with RUNX1-S291fsX-transduced *Vav*-Cre–negative *Asxl1*-MT$^{fl/wt}$ (control+RUNX1-S291fsX, white circle) or *Vav*-Cre–positive *Asxl1*-MT$^{fl/wt}$ (KI+RUNX1-S291fsX, black circle; related to Fig. 5 C). **(G and H)** Cell cycle (G) and apoptosis (H) analyses of LSK/CMP/GMP/MEP cells. DAPI/Ki-67 staining and Annexin V staining were used for the analyses of cell cycle and apoptosis, respectively. Control (*Vav*-Cre–negative *Asxl1*-MT$^{fl/fl}$) plus empty vector (n = 4), KI (*Vav*-Cre–positive *Asxl1*-MT$^{fl/fl}$) plus empty vector (n = 3), control plus RUNX1-S291fsX (n = 3), or KI plus RUNX1-S291fsX mutation (n = 3). **(I)** Flow cytometric analysis of BM cells shows that GFP-positive cells are also positive for c-Kit and CD11b (related to Fig. 5 M). Data are presented as mean ± SEM. *, P < 0.05; **, P < 0.01; ***, P < 0.001; ****, P < 0.0001 (Student's t test). All control mice were littermates of KI mice. BMT, bone marrow transplantation; EV, empty vector.

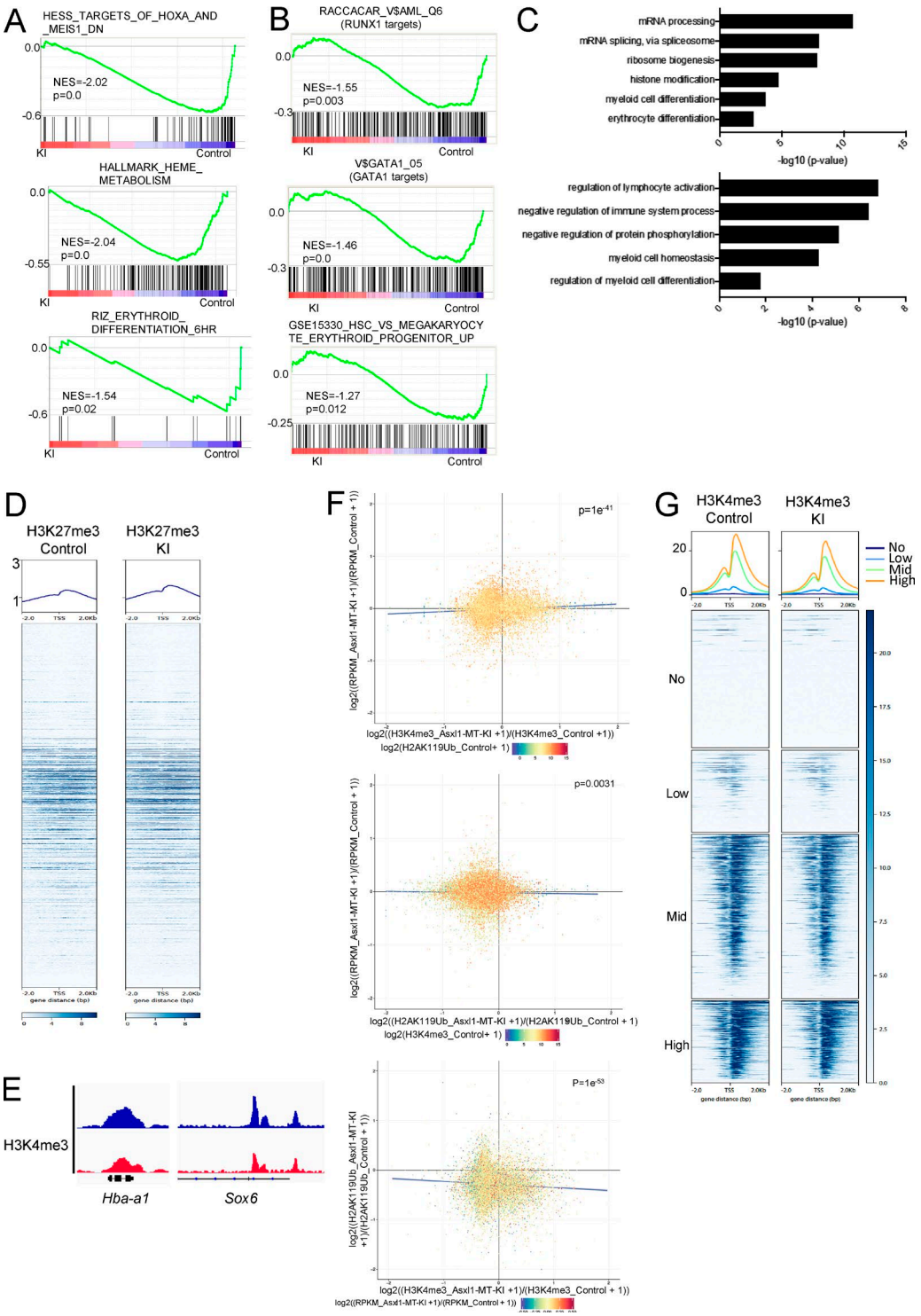

Figure S3. **Transcriptional and epigenetic effects in KI cells. (A and B)** GSEA of c-Kit+ cells (A) and LSK cells (B) determined specific gene sets or pathways that are negatively regulated by expression of Asxl1 mutant (related to Fig. 6 A). KI, *Vav*-Cre–positive *Asxl1*-MT$^{fl/fl}$; control, *Vav*-Cre–negative *Asxl1*-MT$^{fl/fl}$. **(C)** GO biological process enrichment analysis of up-regulated (top) and down-regulated (bottom) genes both in KI and KO cells (related to Fig. 6, B and C). **(D)** Heatmap representation of H3K27me3 ChIP-seq signal around TSSs is shown (related to Fig. 6 E). Control c-Kit+ (left) and KI c-Kit+ (right) cells were used for the analysis. **(E)** Peak result of H3K4me3 ChIP-seq across *Hba* and *Sox6* genes. **(F)** The correlations between the log2-transformed ratio of RNA-sequencing RPKM (KI versus control) and that of H3K4me3 (KI versus control; top) or H2AK119Ub (KI versus control; middle) are shown. H3K4me3 and H2AK119Ub signals were calculated in ± 2.5 kb window around each TSS. H2AK119Ub (top) or H3K4me3 (middle) enrichment in control cells were color coded as indicated. Changes of H3K4me3 and H2AK119Ub were negatively correlated (bottom). The correlations between the log2 transformed ratio of H3K4me3 (KI versus control) and H2AK119Ub (KI versus control) are shown. **(G)** Genes were ranked and divided into four groups based on levels of expression (no expression or low, medium, or high expression). Shown alongside is the genome-wide distribution of H3K4me3 marks across the TSSs of all genes. NES, normalized enrichment score.

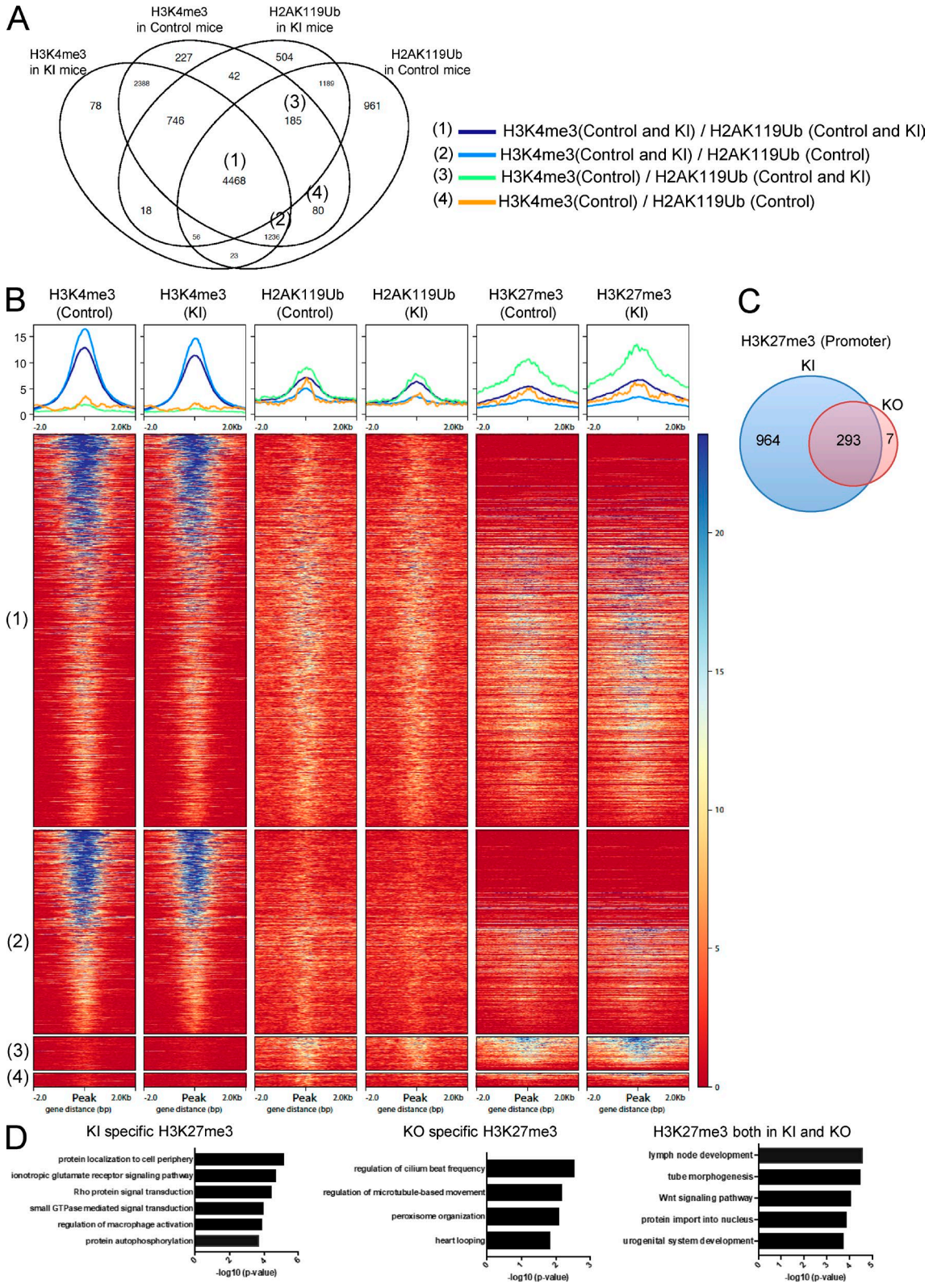

Figure S4. **The effects of mutant expression on histone modification. (A)** Overlap of H3K4me3 and H2AK119Ub peaks in control c-Kit$^+$ cells and KI c-Kit$^+$ cells. The peaks with both H3K4me3 and H2AK119Ub in control cells were divided into four groups: (1) both modifications remained in KI (4,468 peaks), (2) only H3K4me3 remained in KI (1,236 peaks), (3) only H2AK119Ub remained in KI (185 peaks), and (4) both modifications absent in KI (80 peaks). **(B)** Heatmap representation of H3K4me3 (left), H2AK119Ub (middle), and H3K27me3 (right) in groups 1–4. ChIP-seq signals centered on each peak. **(C)** Overlap of genes whose promoters are modified with H3K27me3 in KI c-Kit$^+$ (blue) cells and KO c-Kit$^+$ cells (red). For KO mice, the data from *Mx1*-Cre Asxl1$^{fl/fl}$ mice were used. **(D)** GO biological process enrichment analysis of KI-specific H3K27me3 (top), KO-specific H3K27me3 (middle), and common H3K27me3 peaks in both KI and KO (bottom).